Journal of Materials Research and Technology 42 (2026) 5813–5824

Contents lists available at ScienceDirect

Journal of Materials Research and Technology

journal homepage: www.elsevier.com/locate/jmrt

Effect of aging on the properties of PEEK fabricated via fused filament fabrication

Erica Billè [a,*], Alessandro Gambitta [b], Alex Lanzutti [a], Alfredo Rondinella [a], Francesco Sordetti [a], Marco Sortino [a], Giovanni Totis [a], Emanuele Vaglio [a]

[a] Polytechnic Department of Engineering and Architecture, University of Udine, Via delle Scienze 206, Udine, 33100, Italy
[b] Elettra-Sincrotrone Trieste, Area Science Park, Basovizza, Trieste, 34149, Italy

ARTICLE INFO

Keywords:
Additive manufacturing
PEEK
Fused filament fabrication
Aging

ABSTRACT

Polyether ether ketone (PEEK) is a high-performance thermoplastic widely used in aerospace, biomedical, automotive, and nuclear sectors owing to its excellent mechanical, thermal, and chemical stability. Fused filament fabrication (FFF) has recently emerged as an accessible additive manufacturing route for PEEK, enabling the production of customized components with complex geometries. However, the long-term aging behavior of FFF-printed PEEK remains poorly understood. Environmental stressors such as UV radiation, humidity, and temperature can induce chain scission, oxidation, and crystallinity variations, ultimately affecting structural integrity and durability. Moreover, intrinsic microstructural features of FFF, including interlayer porosity and filament orientation, may amplify these degradation phenomena compared to bulk PEEK.

This study investigates the effects of controlled environmental aging — UV exposure, hygrothermal conditions, and combined UV + hygrothermal treatments — on the mechanical, chemical, and tribological properties of FFF-printed PEEK. Mechanical (tensile, hardness, and wear), chemical (FTIR, EDXS), and morphological (SEM) analyses were employed. UV aging induced marked surface photo-oxidation and cracking, while unexpectedly enhancing tensile strength and ductility, indicating damage confined to the outer surface. Hygrothermal aging caused no significant oxidation but increased crystallinity and stiffness, with limited effects on tensile properties and a moderate reduction in wear resistance. The combined UV+HT treatment produced the most severe surface oxidation and erosion together with the highest strength and ductility, but the poorest tribological performance. Overall, the results demonstrate a decoupling between surface degradation and bulk mechanical behavior, revealing new pathways for tuning performance and guiding protection strategies for FFF-printed PEEK.

1. Introduction

Polyether ether ketone (PEEK) is a semicrystalline thermoplastic polymer belonging to the polyaryl ether ketone (PAEK) family [1]. Its molecular structure endows PEEK with a unique combination of properties, including high mechanical strength, thermal and chemical stability [2,3], wear and radiation resistance [4], and excellent biocompatibility [5]. PEEK has a melting temperature of approximately 340 °C, a glass transition temperature of 143 °C, and maintains its mechanical properties up to around 260 °C, making it suitable for high-performance applications [6]. These characteristics have promoted its use in advanced sectors [7], such as biomedical, aerospace, automotive, and nuclear industries, where lightweight, strong, and stable materials are required under extreme conditions [8].

PEEK components can be fabricated using various conventional methods, including machining, injection molding, extrusion, and compression molding. While well-established, these techniques have limitations, such as high mold costs, long production times, and design restrictions. In recent years, additive manufacturing has expanded the possibilities for PEEK applications, allowing the production of complex geometries and customized components [1]. Among the adopted technologies, Selective Laser Sintering (SLS), Direct Ink Writing (DIW), and Fused Filament Fabrication (FFF) stand out. SLS, although promising, is limited by high costs, low part density, and powder recycling challenges [9]. DIW suffers from low mechanical strength and requires complex post-processing. In contrast, FFF offers process simplicity, lower

* Corresponding author.
E-mail address: erica.bille@uniud.it (E. Billè).
URL: https://orcid.org/0009-0009-4809-0045 (E. Billè).

https://doi.org/10.1016/j.jmrt.2026.04.142
Received 23 January 2026; Accepted 16 April 2026
Available online 23 April 2026

costs, and ease of use, making it the most widely employed technique for PEEK in research, production, and educational settings [1].

PEEK is increasingly processed through FFF for the production of complex and high-performance components due to its excellent mechanical properties. In particular, previous studies have shown that FFF-manufactured PEEK can exhibit remarkable static mechanical performance [10] as well as good fatigue resistance [11], making it suitable for demanding engineering applications.

However, the mechanical performance and overall quality of FFF-produced PEEK components are strongly influenced by the processing conditions [12]. Variations in printing parameters—such as nozzle temperature, printing speed, layer thickness, and raster orientation—can significantly affect interlayer bonding, porosity, and crystallinity, leading to considerable differences in the mechanical behavior of the printed parts. Moreover, differences in printing systems and processing strategies can further contribute to variability in the final properties of FFF-manufactured PEEK components.

Although many studies have investigated the influence of FFF printing parameters on the final properties of PEEK components, aging remains a less explored aspect. Understanding aging is crucial for evaluating long-term reliability and performance.

Polymer aging is a complex process influenced by environmental factors such as UV radiation, humidity, and temperature, which lead to photo-oxidation, hydrolysis, and chain scission. Common consequences include loss of mechanical strength, embrittlement, yellowing, and changes in crystallinity. Studies on conventional polymers such as polystyrene (PS) and polyvinyl chloride (PVC) have shown that UV exposure induces radical formation [13], C–H bond cleavage, and the formation of oxygen-containing groups (C=O, C–O), leading to surface degradation, reductions in mechanical performance [14,15], as well as creep and color changes [16]. Similar effects have been observed in polycarbonate (PC) [17]. In polyolefins, such as polypropylene (PP), polyethylene (PE), and thermoplastic polyurethane (TPU), aging is accelerated by combined heat and radiation, causing photo-oxidation and abrasion that lead to microcracks and microplastic formation [18,19]. Bioplastics, including polylactic acid (PLA), are also sensitive to moisture and light, which promote hydrolysis and photo-oxidation, resulting in significant reductions in molecular weight and mechanical strength [20,21]. These phenomena also affect composites, which may exhibit delamination, swelling, and polymer chain scission [22].

In additive manufacturing polymers, such as PLA, PETG and ABS, UV [23,24] and hygrothermal [25] aging effects are often amplified by the layer-by-layer structure, which introduces weaker interlayer bonding and variations in crystallinity.

Several studies have investigated the response of pure PEEK to different aging conditions, including gamma irradiation [36] and chemical exposure [37]. In this work, the focus is placed on environmentally relevant aging conditions, UV, hygrothermal, and thermal exposure. Table 1 summarizes the main literature studies addressing these conditions, reporting processing routes, aging parameters, characterization techniques, and key findings. Environmental and thermal aging can induce photo-oxidation, hydrolysis, and chain scission, leading to changes in crystallinity, embrittlement, and reductions in mechanical performance. For conventional PEEK, UV exposure has been shown to promote oxidation and surface degradation, increasing variability in mechanical response [26]. Similarly, stress- and temperature-dependent embrittlement has been observed in extruded PEEK sheets [27]. Hygrothermal aging affects filament properties and print quality, increasing porosity and reducing density, hardness, and tensile strength [1]. Moisture absorption also leads to reductions in tensile and compressive properties in injection-molded PEEK [32] and minor modulus decreases in FFF-printed samples [33]. Thermal aging induces crosslinking and secondary crystallization, which increase stiffness but reduce ductility and long-term thermal stability [6]. Thermo-oxidative aging of extruded and stretched PEEK initially increases strength due to crosslinking, then leads to degradation and reduced crystallinity at higher temperatures [29]. Long-term cyclic and thermal exposure in FFF-printed PEEK shifts crystallization and increases embrittlement [34]. Combined thermo-oxidative and humidity exposure decreases crystallinity and elongation, increases brittleness, and degrades dielectric properties [8]. Chain scission and crosslinking induced by thermal aging also reduce elongation while increasing dielectric losses [30]. Injection-molded PEEK shows improved stiffness and strength under thermal aging, but toughness and impact resistance decrease, while tribological performance may improve [31]. In FFF-printed PEEK, anisotropy introduced by layer orientation strongly influences flexural behavior, whereas moisture uptake has limited effect [35]. Despite pure PEEK's resistance to environmental stressors, most studies focus on bulk or sheet samples produced via conventional processes. Data on FFF-printed components remain sparse, and the effects of combined aging conditions on their chemical, mechanical, and morphological properties are not fully understood. The present work addresses this knowledge gap by systematically investigating UV, thermal, and hygrothermal aging of FFF-PEEK. Chemical changes are analyzed via FTIR and EDXS, mechanical properties via tensile, hardness, and wear tests, and surface morphology via SEM, providing a comprehensive understanding of aging mechanisms in additively manufactured PEEK.

2. Materials and methods

2.1. Sample design and printer settings

In the present study, PEEK filament (Intamsys, 1.75 mm in diameter) was employed for specimen fabrication. Printing was carried out using an Intamsys Funmat HT printer, equipped with a closed build chamber, which ensured the maintenance of a thermally stable environment throughout the entire manufacturing process. The processing parameters, reported in Table 2, were selected according to the optimal conditions identified in the work of Billè et al. [12].

Wear specimens were produced according to the geometrical dimensions reported by Regis et al. [38], while tensile specimens were fabricated following the ISO 527-2:2012 standard [39]. The specimen geometry was based on type 5 A; however, a thickness of 4 mm was adopted to accommodate the requirements of the additive manufacturing process and to ensure sufficient interlayer bonding and structural integrity. All specimens were manufactured using the same printing parameters, ensuring internal consistency of the results. A full factorial experimental design was adopted in this study. A total of twelve specimens were prepared for each geometry, corresponding to three replicates for each aging condition in addition to the as-printed reference. The number of specimens is considered sufficient to ensure repeatability and statistical reliability. The geometrical details of the specimens are shown in Fig. 1.

All specimens were fabricated with a horizontal orientation on the build platform, with the larger surface of the specimen in direct contact with the platform. Wear specimens were polished to minimize the influence of printing-induced surface irregularities on the trajectory of the wear test probe. Three distinct aging protocols were applied. In the first, specimens were exposed to ultraviolet (UV) radiation at 300–400 nm within a suntest XLS+ chamber for 168 h, with an intensity of 65 W/m^2. This exposure corresponds approximately to 6–8 months of outdoor UV exposure, assuming a typical monthly UV dose of 5–7 MJ/m^2. In the second, hygrothermal aging (HT) was performed by exposing the specimens to a controlled environment at 88 °C and 90% relative humidity (RH) for 168 h in a climatic chamber (model Camera climatica Genviro). In the third protocol, specimens were subjected to a combined aging treatment, consisting of sequential exposure to both UV and hygrothermal conditions (UV+HT). In Fig. 2, the aged tensile specimens and the effect of each aging treatment on their color can be observed. Accelerated aging durations reported in the literature for PEEK vary widely depending on the applied environmental conditions and the investigated degradation mechanisms, ranging from a few hours to several weeks, as summarized in Table 1. In the present study,

Table 1
Summary of literature studies on pure PEEK aging, reporting processing methods, aging conditions (UV irradiation, thermal and hygrothermal exposure), key parameters (temperature, relative humidity, wavelength, exposure time and environment), characterization techniques and main findings. *Acronyms used:* TOA = Thermo-Oxidative Aging; HT = Hygrothermal; RH = Relative Humidity; T = Temperature; t = Time; E = Energy dose; σ = Applied stress; Tens. = Tensile; Comp. = Compression; 3PB = Three-point bending; diel. = dielectric; ζ = zeta potential; resist. = resistivity; diel. str. = dielectric strength; CA = contact angle; MFR = Melt Flow Rate.

Ref.	Proc.	Aging conditions	Tests	Key results
[26]	Injection molding	UV, $\lambda > 300$ nm, T = 60 °C, t = 0–382 h	FTIR, DSC, μ-indent.	Oxidation leads mainly to crosslinking, forming aromatic products; crystallinity and modulus increase with an oxidized surface layer.
[27]	Extruded sheet	UV, λ = 250–400 nm, T = 80–130 °C, E = 3.47×10^4 J/cm^2, σ = 0–4.68 MPa, vacuum	FTIR, XPS, DSC, μ-indent., Tens.	Embrittlement depends on stress and temperature, showing a balance between chain scission and crosslinking.
[28]	FFF	UV, λ = 340 nm, 0.83 W/m^2, t = 170–350 h	3PB, Tens., DMA, DSC, TGA	Reprocessing of UV-aged PEEK is feasible with limited degradation of properties.
[1]	Filament (FFF)	HT, T = 25 °C, RH = 60%, t = 0–72 h	SEM, Tens., dens., hard., MFR, microscopy	Moisture absorption degrades print quality, increasing porosity and reducing density, hardness and tensile strength.
[6]	Melt-spun fibres	Thermal, T = 250 °C, t = 1–128 d	DSC, FTIR, rheol., TGA, Tens., SEM, UV–Vis	Crosslinking and secondary crystallization increase stiffness but cause embrittlement and reduced thermal stability over time.
[8]	Films	TOA, T = 250 °C + cyclic HT, T = 90 °C, RH = 90%, t = 24–170 h	FTIR, SEM/EDS, POM, Tens., DMA, DSC, TGA, UV–Vis, diel.	Combined thermal and humidity aging reduces crystallinity and ductility, increases oxidation, brittleness and dielectric degradation.
[29]	Extrusion/ stretching	TOA (air), T = 170–310 °C, t = 14 d	Tens., FTIR, DSC, TGA	Strength increases up to ~290 °C due to crosslinking, then degradation dominates with reduced crystallinity and stability.
[30]	Sheets	TOA (air), T = 280 °C, t = 0–2852 h	Tens., FTIR, DSC, TGA, diel., ζ, resist., diel. str.	Aging induces chain scission and crosslinking, lowering crystallinity and elongation, increasing dielectric losses and oxidation.
[31]	Injection molding	Thermal, quench from 360 °C, then T = 310 °C, t = 60 min	DSC, 3PB, Charpy, CA, wear	Aging increases stiffness and strength but reduces toughness; tribological performance improves.
[32]	Injection molding	HT, T = 70 °C, RH = 85%	Gravim., Tens., Comp., SEM	Moisture follows Fickian diffusion; tensile strength strongly decreases, modulus slightly affected.
[33]	FFF	HT, T = 70 °C, RH = 85%, t = 1000 h	TGA, FTIR, DSC, DMA, Tens., SEM	Slight modulus reduction, negligible changes in Tg, crystallinity and tensile strength.
[34]	FFF	Thermal, T = 250 °C, t = 2–10 h; long-term T = 200 °C, t = 10–30 d; cyclic 100 cycles at 200 °C (24 h)	DSC, Tens.	Aging shifts crystallization and increases embrittlement after prolonged exposure.
[35]	FFF	HT, T = 132 °C, RH = 100%, P = 1.2 atm, t = 5 h; prior annealing up to 200 °C	3PB, SEM, water abs.	Accelerated aging degrades mechanical properties due to crystal structure defects; flexural behavior is strongly dependent on build orientation, while moisture uptake shows negligible influence.

Table 2
Fused filament fabrication printing parameters.

Parameters	Values	Units
Nozzle temperature	420	°C
Nozzle speed	40	mm/s
Layer thickness	0.1	mm
Nozzle diameter	0.4	mm
Bed temperature	145	°C
Chamber temperature	90	°C
Infill pattern	+45/-45	°
Infill density	100	%
Number of perimeters	1	wall
Number of top/bottom solid layers	3	layer

an aging duration of 168 h was selected as a representative exposure time capable of inducing measurable variations in the material properties while maintaining a feasible experimental timeframe.

The effects of the three aging treatments were assessed by evaluating the mechanical properties of the specimens, together with microstructural and chemical analyses performed by Scanning Electron Microscopy (SEM), Fourier-Transform Infrared Spectroscopy (FTIR), and Energy-Dispersive X-ray Spectroscopy (EDXS). For reference, the same characterization procedures were also carried out on as-printed specimens, enabling direct comparison with the aged samples.

2.2. Chemical analysis

A chemical analysis was carried out to gain deeper insight into the behavior of the materials during the printing process, which directly affects the final properties of the samples. To assess possible modifications in the polymer composition induced by the FFF process, Attenuated Total Reflectance Fourier-Transform Infrared Spectroscopy (ATR-FTIR) was employed. Measurements were performed using a Thermo Fisher Scientific Nicolet iS™ 50 spectrometer. Infrared spectra were collected at a resolution of 2 cm^{-1} over the spectral range of 500–4000 cm^{-1}, with 32 scans recorded for each measurement.

The chemical composition was determined by Energy-Dispersive X-ray Spectroscopy (EDXS) using a system integrated into the Scanning Electron Microscope (SEM). For each aging condition, EDXS measurements were performed at three locations on one tensile specimen and at eight locations on different wear specimens outside the wear tracks, followed by an additional eight measurements within the wear tracks on different specimens.

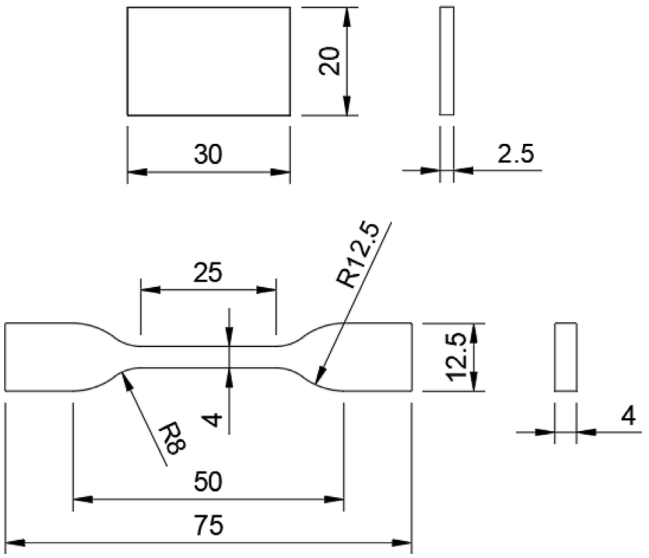

Fig. 1. Geometries of the specimens used in the wear and tensile tests (dimensions in mm). Top: wear test specimen; bottom: tensile test specimen.

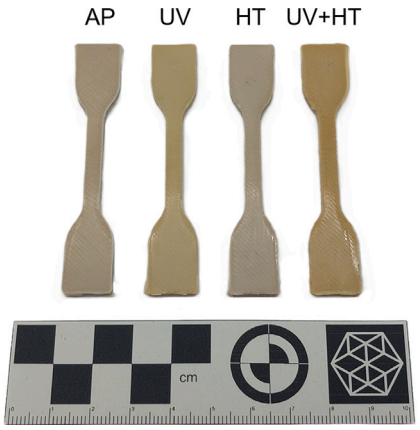

Fig. 2. Aged tensile specimens.

2.3. Surface morphology

The samples were examined using a Zeiss EVO 40 scanning electron microscope (SEM) for surface characterization. For each aging condition, the upper surfaces of three specimens were analyzed at an accelerating voltage of 20 kV. Surface images were acquired at magnifications of 50×, 200×, and 1000× for the tensile specimens, and at 50× and 200× for the surfaces and wear tracks of the wear specimens.

2.4. Mechanical testing

Wear tests were carried out using a CTER UMT-3 tribometer in a ball-on-flat configuration. The counterbody consisted of an Al_2O_3 sphere with a diameter of 1/8", in accordance with the study by Regis et al. [38]. The instrument was equipped with a biaxial load cell with a maximum capacity of 10 N, and a normal load of 7 N was applied on the pin. Tests were performed in reciprocating mode with a 10 mm stroke at 1 Hz. The initial test duration was set to 3600 s, corresponding to a total sliding distance of 72 m. For each configuration, three specimens were tested to ensure statistical significance of the results.

The wear rate was determined from the volumetric loss, measured using stylus profilometry. The wear rate (K) was calculated as: $K = V_a/(S \cdot F_z)$ where V_a is the removed material volume, S the sliding distance, and F_z the applied normal load [40].

The wear tracks were analyzed using a Sensofar S-Neox non-contact microscope operating in confocal mode, equipped with a Nikon EPI 20× objective (pixel size: 0.34 μm/pixel). An area of 2.01 × 1.68 mm^2 was scanned, and the corresponding wear track profiles were extracted using Sensofar SensoVIEW software.

Tensile tests were conducted on dedicated specimens using a Shimadzu AGX-V2 universal testing machine equipped with a 5 kN load cell, following the ISO 527-1:2012 standard. The crosshead speed was initially set to 1 mm/min to determine the Young's modulus (E), and subsequently increased to 5 mm/min.

Hardness measurements were performed using a DuraJet G5 device equipped with a 5 mm spherical indenter, under an applied force of 358 N, following the EN ISO 2039-1 standard [41]. The measurements were carried out on the surfaces of the specimens after the wear test, in areas located outside the wear tracks. Specifically, three indentations were made in the central region of each sample and three in the outermost area.

All tests were performed under standard ambient conditions.

For each tensile test, three repetitions were performed for each aging condition to ensure sufficient repeatability. For the tribological wear and hardness tests, three measurements were taken on each specimen, resulting in a total of nine repetitions per aging condition. Statistical significance among the investigated conditions was evaluated using one-way analysis of variance (ANOVA) implemented in MATLAB ($p < 0.05$). When significant differences were detected, post-hoc multiple comparisons were performed using the Tukey–Kramer method to identify pairwise differences between groups. All statistical analyses were performed using MATLAB. The reported p-values indicate whether differences between aging states were statistically significant. This approach provides a robust framework for interpreting the experimental results and ensures the reproducibility and transparency of the data analysis.

3. Results

3.1. Chemical analysis

Fig. 3 presents the normalized FTIR spectra of aged and non-aged PEEK, with the main vibrational bands indicated. The assignment of these bands to their respective vibrational modes is reported in Table 3. The spectra show differences between the as-printed material (AP) and the samples subjected to UV (UV), hygrothermal (HT) and combined UV+hygrothermal (UV+HT) aging. In all cases, the characteristic absorption bands of PEEK are observed, with no additional bands appearing after aging [33].

The AP sample exhibits the typical spectrum of PEEK, characterized by well-defined peaks corresponding to aromatic C–H stretching at 3065 cm^{-1}, aliphatic methylene vibrations between 2920 and 2850 cm^{-1}, the carbonyl band at 1648 cm^{-1}, and the aromatic ring skeletal vibrations between 1595 and 1488 cm^{-1} [44,47]. After UV exposure, the spectra show an increase in the intensity of the broad band around 3400 cm^{-1} in the 4000–2000 cm^{-1} region. The aromatic band at 3065 cm^{-1} and the aliphatic bands between 2920 and 2850 cm^{-1} also exhibit higher intensity compared with the AP condition. In the fingerprint region, the carbonyl band at 1648 cm^{-1} becomes broader and more intense. The HT-aged sample exhibits more limited spectral variations. The aromatic bands between 1595 and 1488 cm^{-1} appear slightly more intense, and a small increase in the intensity of the C=O and C–O–C bands is observed. In the 3600–3200 cm^{-1} region, no noticeable increase in band intensity is detected. The UV+HT aged sample shows the most pronounced spectral variations. The broad band in the 3600–3200 cm^{-1} region increases markedly in intensity. Changes in the intensity and shape of the aromatic and aliphatic C–H bands are also observed. In the fingerprint region, the carbonyl band at

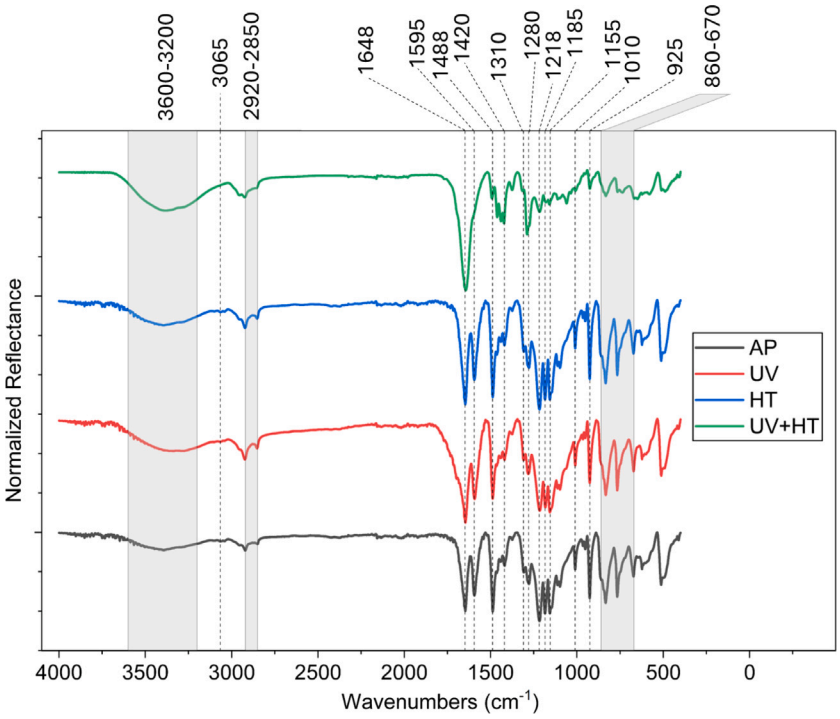

Fig. 3. Normalized FTIR spectra of aged and non-aged PEEK.

Table 3
Summary of the main FTIR vibrational bands identified in additively manufactured PEEK and the related vibrational modes.

Position [cm^{-1}]	Vibrational Mode	Reference
3600–3200	O–H stretching	[42]
3065	CH-stretching vibration of the aromatic rings	[42]
2920–2850	Aliphatic methylene group vibrations	[42]
1648	C=O stretching (ketone group)	[43]
1595, 1488, 1420	Skeletal vibration of phenyl ring	[44]
1310	Bending motion of the ketone group (C–C(=O)–C)	[45]
1280, 1218, 1185	Asymmetric stretching of the diphenyl ether group C–O–C	[8]
1155, 1010	C–H bending (aromatic)	[44]
925	Diphenyl ether group vibration	[46]
860–670	Out-of-plane bending of aromatic C–H	[45]

Table 4
Carbon/Oxygen weight ratio measured on tensile and wear specimens.

Sample	C/O [–]
As-printed	3.67 ± 0.20
UV aging	2.61 ± 0.17
HT aging	3.51 ± 0.27
UV+HT aging	2.85 ± 0.23

1648 cm^{-1} appears broader and slightly asymmetric. Variations in the C–O–C bands between approximately 1150 and 1200 cm^{-1} and in the bands between 900 and 800 cm^{-1} are also detected.

The EDXS analysis was performed to evaluate the surface chemical composition of the samples after the different aging treatments. The mean carbon-to-oxygen (C/O) weight ratios measured for each condition are reported in Table 4.

A clear decrease in the C/O ratio is observed after UV aging, indicating an increase in oxygen content at the sample surface. In contrast, the HT-aged samples exhibit values comparable to those of the as-printed condition, suggesting that hygrothermal exposure alone induces only limited oxidation. The combined UV+HT treatment results in intermediate C/O values between the AP and UV conditions.

Statistical analysis confirms that both UV and UV+HT aging lead to a significantly higher oxygen content compared with the as-printed samples ($p < 0.001$). A significant difference is also observed between the UV and UV+HT conditions ($p < 0.006$). The slightly higher C/O ratio measured for the UV+HT samples indicates that their oxygen content is somewhat lower than that of the UV-aged samples.

3.2. Surface morphology

The surfaces of the samples subjected to tensile and wear tests were analyzed by scanning electron microscopy (SEM), as shown in Figs. 4 and 5. In the AP sample, the surface appears relatively homogeneous and free of macroscopic defects, with well-defined and regular deposition lines. In Fig. 5(a), these lines are clearly visible, and a localized defect can be observed on the surface. For the UV-aged sample, the surface remains generally smooth but appears less homogeneous than the AP condition. Altered regions and small point-like defects are visible. More pronounced cracks are observed along the deposition lines (Fig. 5(b)). Scattered micro-pores are also detected and are preferentially oriented along the printing direction. The edges of the cavities appear irregular and rough. In the HT-aged sample, the surface shows more pronounced micro-grooves and an overall wavy morphology. At higher magnifications, the microstructure appears compact and relatively uniform, and no evident micro-porosity is observed.

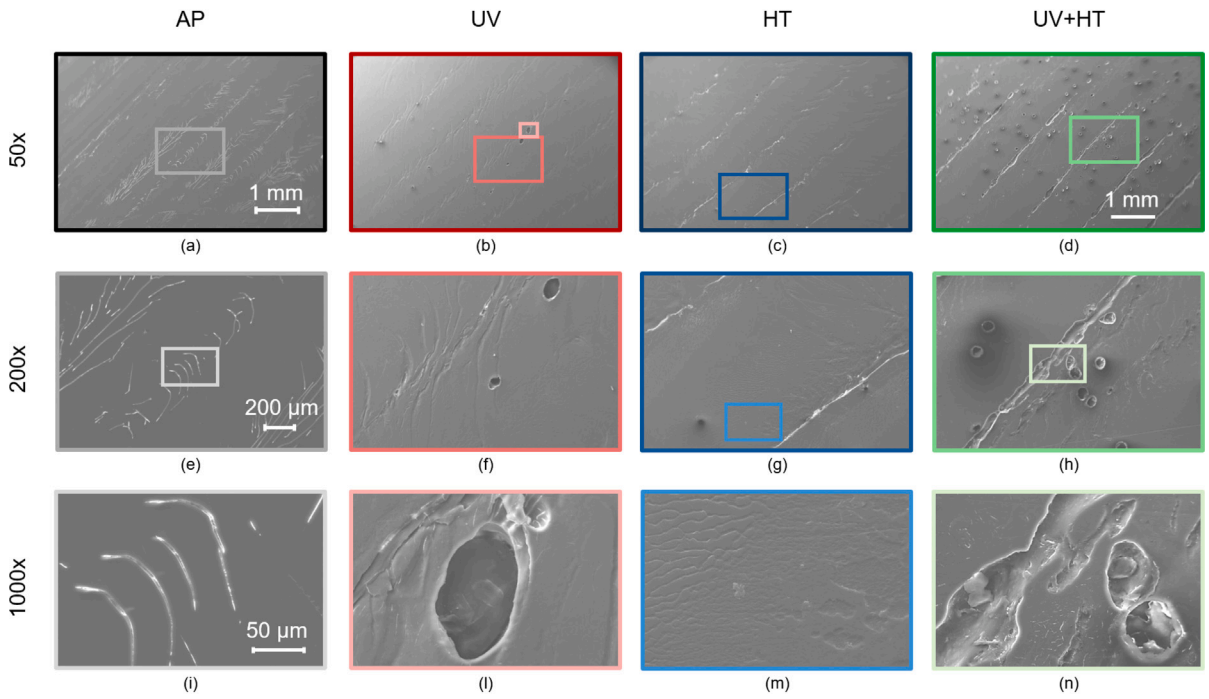

Fig. 4. SEM micrographs of the tensile specimen surfaces. Columns correspond to the different aging treatments applied, while rows represent the various magnification levels.

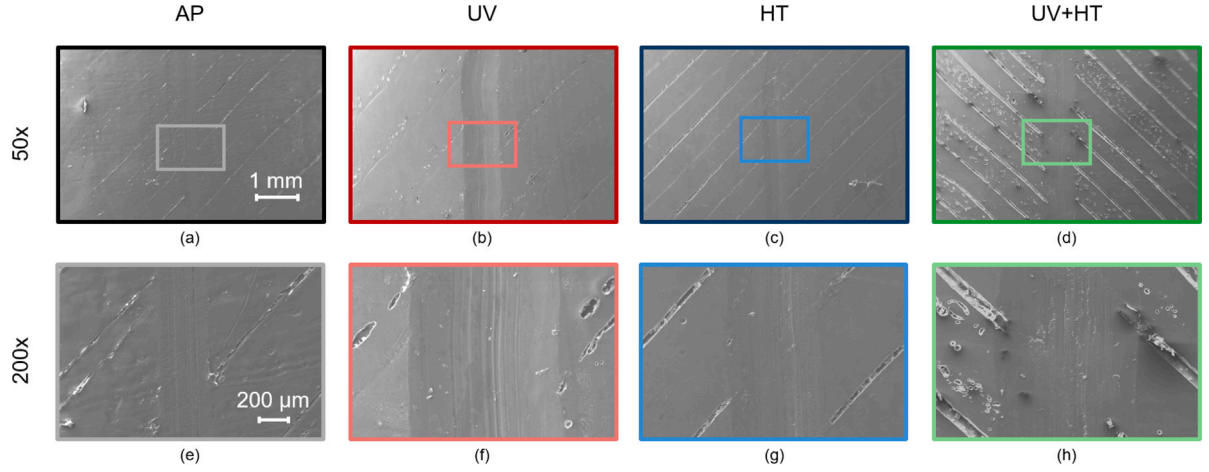

Fig. 5. SEM micrographs of specimen wear surfaces. Columns indicate the applied aging treatments, while rows correspond to different magnifications.

The UV+HT sample exhibits the most pronounced surface alterations. Numerous defects such as micro-craters and eroded areas are visible. The deposition lines appear more irregular than in the other samples, and cavities and micro-voids are distributed along the deposition paths.

3.3. Mechanical testing

The results of the tensile and hardness tests performed on FFF-printed PEEK samples in the AP condition and after the different aging treatments are summarized in Table 5. The statistical distribution of the mechanical properties is shown in Fig. 6, while the representative stress–strain curves are reported in Fig. 7.

All samples exhibit the typical mechanical response of semicrystalline PEEK, characterized by an initial linear elastic region followed by plastic deformation up to failure. The initial portions of the stress–strain curves are nearly overlapping for all conditions.

Statistical analysis shows that aging has a significant effect on the ultimate tensile strength (UTS) ($p < 0.05$), meaning that at least one aging condition produces a measurable change in strength. In contrast, the elastic modulus does not vary significantly among the tested conditions ($p > 0.05$), indicating that the bulk stiffness of the material remains essentially unchanged. The maximum elongation at break is close to the significance threshold ($p \approx 0.05$), suggesting only minor differences among the conditions.

Table 5
Mechanical properties values: ultimate tensile strength (UTS), elastic modulus (E), maximum elongation percentage (%EL) and hardness (HB).

Sample	UTS [MPa]	E [MPa]	%EL [%]	HB [MPa]
As-printed	55.6 ± 1.1	1858 ± 97	6.4 ± 0.1	276 ± 16
UV aging	59.4 ± 1.1	1787 ± 160	6.7 ± 0.5	281 ± 51
HT aging	56.6 ± 2.2	1872 ± 73	6.6 ± 0.2	263 ± 36
UV+HT aging	60.5 ± 1.1	1836 ± 53	7.2 ± 0.2	223 ± 60

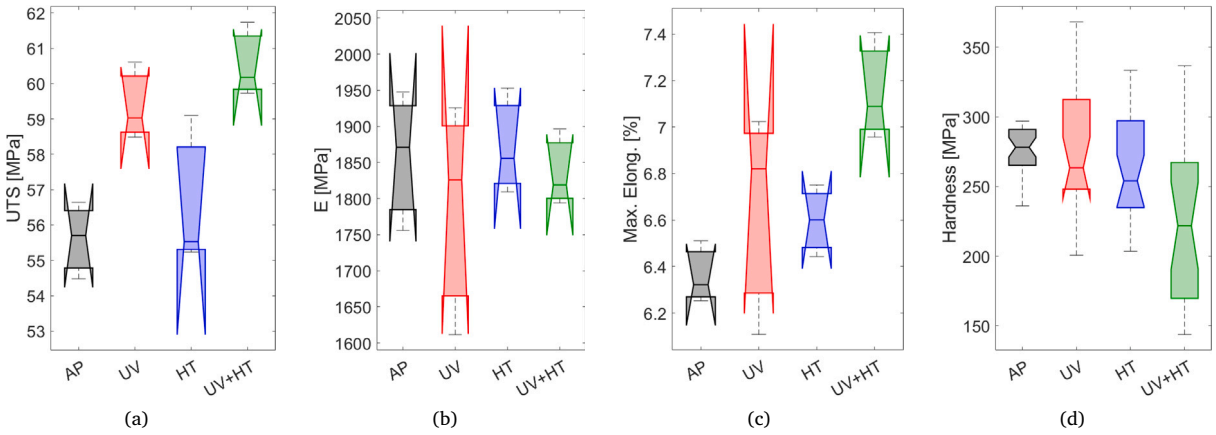

Fig. 6. Effect of the different aging on (a) Ultimate Tensile Strength, (b) Elastic modulus, (c) Maximum Elongation Percentage and (d) Hardness.

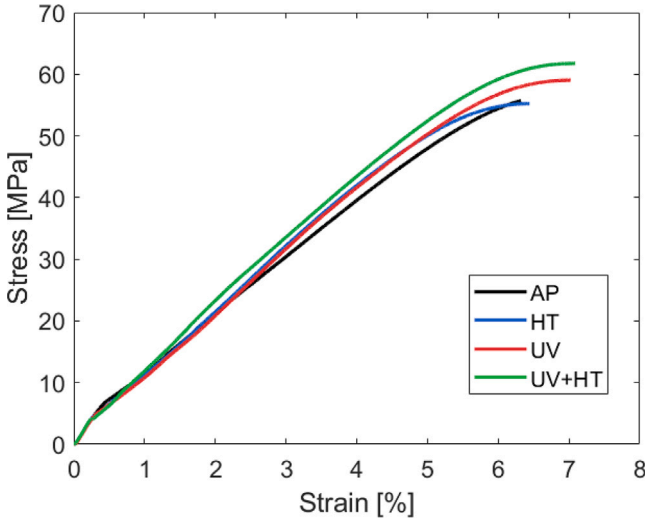

Fig. 7. Tensile stress–strain curves of PEEK samples subjected to different aging conditions.

As reported in Table 5, UV aging leads to an increase in tensile strength compared with the as-printed condition. The HT-aged samples exhibit tensile properties comparable to the AP samples, while the combined UV+HT treatment results in the highest tensile strength and elongation at break among the investigated conditions. In all cases, the elastic modulus remains within a similar range.

Regarding hardness, statistical analysis indicates that the aging conditions significantly influence the measured values ($p < 0.05$). While the UV-aged samples show hardness values comparable to those of the as-printed material, the HT treatment produces a slight reduction. The lowest hardness values are observed for the UV+HT condition, indicating a softening of the surface after the combined aging treatment.

3.4. Tribological behavior

The results of wear test are summarized in Table 6, where is indicated the values of removed material volume (V_a) and wear coefficient (K). Fig. 8 shows the transverse profiles of the wear tracks obtained for the samples under the different aging conditions, while Fig. 9 presents the corresponding 3D topographical maps.

The as-printed (AP) samples exhibit the best tribological performance, characterized by the lowest wear volume and wear coefficient among all tested conditions.

Table 6
Wear tests values: removed material volume (V_a) and wear coefficient (K).

Sample	V_a [mm^3]	K [10^6 mm^3/Nm]
As-printed	0.004 ± 0.007	14 ± 8.8
UV aging	0.197 ± 0.071	390 ± 140
HT aging	0.030 ± 0.025	60 ± 50
UV+HT aging	0.299 ± 0.160	590 ± 330

After UV aging, the wear behavior deteriorates markedly. The wear track becomes wider and deeper, indicating a substantial increase in material removal compared with the AP condition. The HT-aged samples show an intermediate wear response. Although the wear track is deeper than that of the AP samples, it remains significantly less pronounced than that observed after UV aging. The most severe wear behavior is observed for the UV+HT condition. In this case, the wear track reaches the greatest depth and displays the widest profile among the tested samples, indicating the highest level of material removal. EDXS measurements performed inside the wear tracks reveal a lower oxygen content compared with the surrounding surface for both UV and UV+HT conditions (Fig. 10), suggesting that the reciprocating wear process removes the oxidized surface layer generated during aging.

4. Discussion

4.1. Chemical degradation mechanisms

The FTIR spectral changes observed after aging provide insight into the chemical degradation mechanisms affecting additively manufactured PEEK. The increase in the broad band around 3400 cm^{-1} observed after UV exposure can be attributed to the formation of hydroxyl groups generated during photo-oxidation and to the adsorption of moisture on the oxidized surface. Similar spectral features have been reported in previous studies on UV-aged PEEK and other aromatic polymers [42,48]. The increase in the intensity of the aromatic and aliphatic C–H bands may be associated with polymer chain scission processes induced by ultraviolet radiation. Photodegradation can generate shorter molecular segments with higher vibrational mobility, which may lead to changes in band intensity in the high-frequency region [49]. In addition, the broadening of the carbonyl band at 1648 cm^{-1} suggests the formation of additional oxidized species such as secondary carbonyls or carboxylic groups. In contrast, the more limited spectral variations observed after hygrothermal aging indicate that this treatment induces weaker chemical modifications. The absence of a significant increase in the O–H band suggests that oxidation processes are relatively limited under these conditions. The slight increase in the

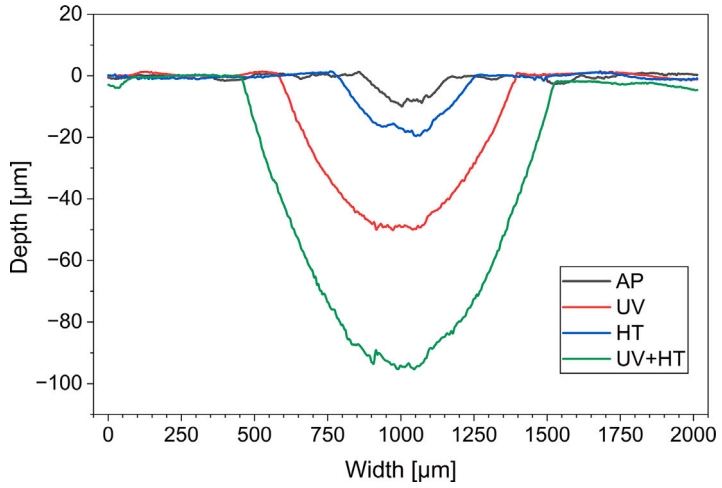

Fig. 8. Profiles of the wear traces.

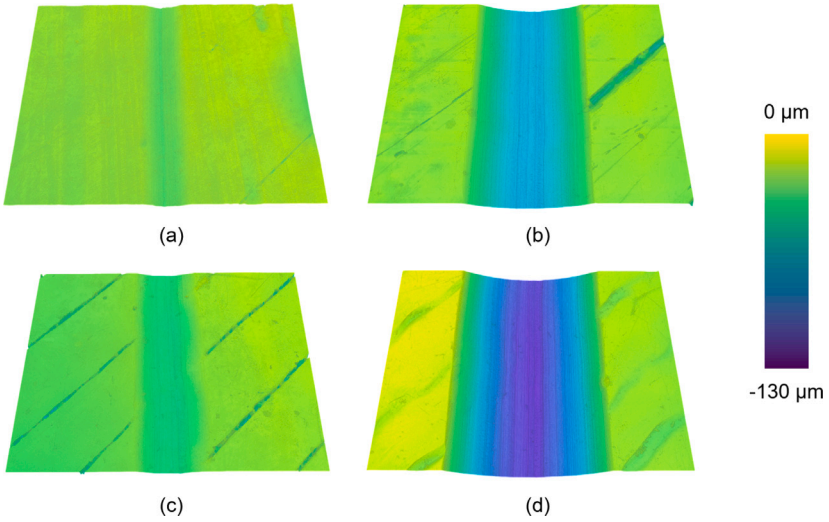

Fig. 9. Wear traces after (A) AP, (B) UV, (C) HT, and (D) UV+HT aging. The color bar indicates depth.

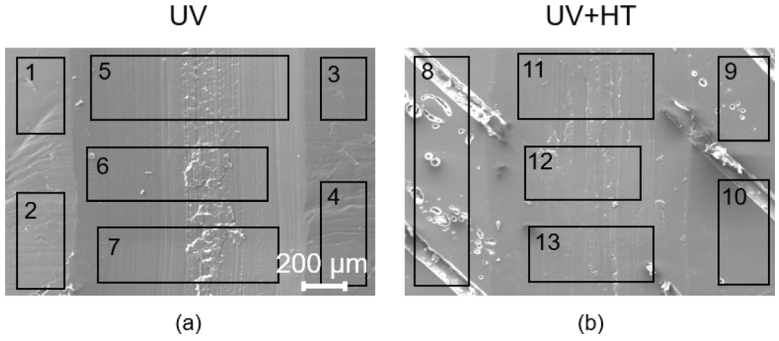

Fig. 10. EDXS analysis of the UV (a) and UV+HT (b) aged samples within and outside the wear track. Points 1–7 correspond to the UV condition: areas 1–4 are located outside the wear track (O = 27.88 ± 1.66 wt%), while areas 5–7 are located inside the wear track (O = 21.48 ± 0.75 wt%). Points 8–13 correspond to the UV+HT condition: areas 8–10 are outside the wear track (O = 26.54 ± 0.52 wt%), whereas areas 11–13 are inside the wear track (O = 21.71 ± 0.60 wt%).

intensity of aromatic and carbonyl bands may instead reflect structural rearrangements occurring within the semicrystalline polymer matrix. Elevated temperature can increase chain mobility within the amorphous regions, promoting molecular reorganization and potentially increasing the degree of crystallinity [8], a mechanism inferred from literature rather than experimentally verified in the present work. The combined UV+HT condition produces the most pronounced spectral modifications. The strong increase in the O–H band together with the broadening of the carbonyl peak indicates that photo-oxidation remains the dominant degradation mechanism. At the same time, changes observed in the C–O–C and aromatic deformation bands suggest that the hygrothermal environment may contribute to additional structural

rearrangements within the polymer matrix. The coexistence of these effects points to a synergistic interaction between photodegradation and thermally activated molecular mobility in the aged material.

The EDXS results provide insight into the chemical modifications occurring at the surface of the aged PEEK samples. The significant decrease in the C/O ratio observed for the UV-aged samples indicates a clear increase in oxygen content compared with the as-printed material. This behavior is consistent with the occurrence of photo-oxidation processes induced by ultraviolet radiation. During UV exposure, the absorption of high-energy photons by the aromatic backbone of PEEK can generate free radicals through chain scission reactions. These radicals subsequently react with atmospheric oxygen, leading to the formation of oxygen-containing functional groups such as hydroxyls, carbonyls, and peroxides on the polymer surface. The increase in oxygen concentration detected by EDXS therefore reflects the progressive oxidation of the outermost layer of the material. The hygrothermal treatment produces a much smaller variation in the C/O ratio. The HT-aged samples exhibit values close to those of the as-printed condition, indicating that oxidation processes remain relatively limited under these conditions. As reported in the literature, thermo-oxidative reactions in PEEK proceed more slowly and to a lesser extent at moderate temperatures [48]. Consequently, hygrothermal exposure mainly promotes physical or microstructural changes rather than significant chemical oxidation. For the combined UV+HT condition, the oxygen content remains significantly higher than in the AP samples but slightly lower than in the UV-only condition. This behavior suggests that the hygrothermal environment may influence the evolution of the oxidized surface layer formed during UV exposure. Increased molecular mobility at elevated temperature can promote partial structural rearrangement or diffusion processes within the near-surface region, which may slightly reduce the accumulation of oxygen-rich species. The EDXS results are in good agreement with the FTIR analysis presented in the previous section. In particular, the increase in oxygen content observed after UV and UV+HT aging correlates with the intensification of the O–H and C=O absorption bands detected in the FTIR spectra. These complementary observations confirm that photo-oxidation represents the dominant chemical degradation mechanism affecting the surface of PEEK under ultraviolet irradiation.

4.2. Morphological degradation

The SEM observations provide insight into the degradation mechanisms affecting the surface morphology of additively manufactured PEEK under the different aging conditions. The relatively smooth and homogeneous morphology observed in the AP samples reflects the typical surface characteristics of FFF-manufactured PEEK, where the deposition lines produced during the printing process remain clearly visible. After UV exposure, the appearance of cracks, micro-pores and irregular cavities indicates the onset of surface degradation phenomena associated with ultraviolet irradiation. Similar morphological changes have been reported in the literature for polymers subjected to UV-induced photodegradation [17,50]. The formation of pores and cracks is generally attributed to chain scission and oxidation reactions occurring at the polymer surface, which progressively weaken the material and promote the development of micro-defects. The presence of bubbles and surface cavities after UV aging has also been reported by Lin et al. [30]. The HT-aged samples exhibit a different surface evolution. The wavy morphology and the presence of micro-grooves are likely related to the relaxation of residual stresses generated during the additive manufacturing process. Thermal exposure can increase the mobility of polymer chains within the amorphous regions, allowing partial structural rearrangement and stress relaxation. This mechanism may explain the relatively compact and uniform microstructure observed at higher magnifications, as well as the absence of significant micro-porosity. In contrast, the UV+HT condition leads to the most severe surface degradation. The extensive presence of micro-craters, voids and eroded regions suggests that the simultaneous action of ultraviolet radiation and hygrothermal exposure amplifies the degradation processes occurring at the polymer surface. Similar synergistic effects between photodegradation and thermo-oxidative mechanisms have been reported for other polymeric materials [21]. The combined action of oxidative reactions and thermally activated molecular mobility can promote the propagation of cracks and the enlargement of surface defects. These morphological observations are consistent with the chemical modifications identified by FTIR and EDXS analyses. In particular, the increase in oxygen-containing functional groups detected by FTIR and the higher oxygen concentration measured by EDXS after UV and UV+HT aging indicate that photo-oxidation processes occur at the material surface. Such chemical degradation mechanisms can weaken the polymer structure and facilitate the formation of cracks, pores and eroded regions observed in the SEM micrographs.

4.3. Effect of aging on mechanical properties

The mechanical results indicate that the different aging treatments influence the tensile response of FFF-printed PEEK in distinct ways. The nearly overlapping elastic regions observed in the stress–strain curves suggest that the elastic modulus is only marginally affected by aging. This behavior indicates that the bulk stiffness of the material remains largely preserved, which is consistent with the FTIR results showing limited chemical degradation of the polymer backbone [33,51]. The increase in tensile strength observed after UV exposure may be related to surface oxidation processes that lead to the formation of a slightly stiffened superficial layer. Limited crosslinking reactions and oxidative modifications can locally enhance the load-bearing capacity without significantly reducing ductility. In contrast, hygrothermal aging produces only minor changes in tensile properties. The slight increase in elastic modulus observed for the HT samples may be attributed to thermally induced molecular rearrangements, potentially leading to an increase in crystallinity. Elevated temperature can promote polymer chain mobility within the amorphous regions, allowing partial structural reorganization of the semicrystalline structure. The combined UV+HT treatment produces the most pronounced mechanical response, characterized by the highest tensile strength and elongation at break. This behavior suggests a synergistic interaction between UV-induced oxidation and thermally activated molecular rearrangement processes. Hardness measurements reveal a different trend. While UV exposure alone has little effect on surface hardness, the UV+HT condition produces a clear reduction. This softening effect may result from the progressive degradation of the oxidized surface layer combined with thermally activated molecular mobility within the near-surface region.

4.4. Tribological degradation mechanisms

The wear results reveal that aging treatments significantly affect the tribological performance of FFF-printed PEEK. The excellent wear resistance observed for the AP samples reflects the integrity of the original polymer surface and the absence of degradation phenomena. In contrast, UV aging produces a marked deterioration of wear behavior. The significant increase in wear depth and removed material volume indicates that the surface layer becomes more susceptible to mechanical damage. This degradation can be attributed to UV-induced photo-oxidation, which weakens the cohesion of the polymer chains at the surface. The HT condition produces a more moderate deterioration of wear resistance. Although thermal exposure can promote molecular rearrangement and increased crystallinity, the resulting microstructure may become more brittle and less capable of forming a stable transfer film during sliding contact. The most severe wear degradation is observed for the UV+HT condition. The combined action of photo-oxidation and hygrothermal exposure promotes extensive surface damage, leading to deeper wear tracks and higher material removal. These tribological results are consistent with the chemical

and morphological analyses presented earlier. FTIR and EDXS analyses revealed the formation of oxygen-containing functional groups and an increase in surface oxygen concentration after UV and UV+HT aging. SEM observations further showed the presence of micro-cracks, pores and surface defects generated during aging. The combined effect of chemical oxidation and microstructural degradation weakens the surface layer, facilitating crack propagation and material removal during sliding contact. The EDXS measurements performed inside the wear tracks show a lower oxygen concentration compared with the surrounding surface. This observation suggests that the reciprocating motion during the wear test removed the superficial oxidized layer formed during aging, exposing the less oxidized subsurface material.

The high standard deviations, particularly for the wear coefficient, can be attributed to the intrinsic heterogeneity of FFF-printed PEEK. Small variations in deposition parameters and cooling rates lead to local differences in crystallinity and interlayer adhesion, which significantly affect the mechanical and tribological behavior of the material [52]. Moreover, wear tests are inherently sensitive to surface and environmental conditions, further amplifying the scatter in the measured values. In particular, the layer-by-layer nature of FFF introduces interlayer porosity, raster orientation effects, and local variations induced by surface finishing (e.g., polishing), all of which generate spatially heterogeneous mechanical properties. Since tribological response is highly sensitive to local defects and surface discontinuities, these microstructural and morphological inconsistencies directly contribute to the observed dispersion in wear results.

4.5. Overall degradation mechanism of aged PEEK

The results obtained from the different experimental techniques provide a consistent picture of the degradation mechanisms affecting FFF-printed PEEK under the investigated aging conditions. FTIR analysis revealed the progressive formation of oxygen-containing functional groups, particularly hydroxyl and carbonyl species, indicating the occurrence of photo-oxidation processes. This observation was quantitatively supported by EDXS measurements, which showed a clear increase in surface oxygen content after UV and UV+HT exposure. The chemical modifications detected by these techniques are accompanied by morphological changes observed by SEM, where UV-aged surfaces exhibit micro-cracks, pores, and localized defects aligned with the printing direction. These defects weaken the integrity of the surface layer and act as preferential sites for crack initiation and propagation under mechanical loading.

The tensile results indicate that the bulk mechanical response of the material remains relatively stable despite surface oxidation. Slight increases in ultimate tensile strength and elongation at break observed for the UV and UV+HT conditions suggest that aging does not significantly compromise the structural integrity of the bulk material. This behavior highlights the fact that the degradation mechanisms are mainly confined to the superficial layers of the printed components.

In contrast, tribological performance is strongly affected by aging treatments. The severe increase in wear volume and wear coefficient observed for UV and especially UV+HT conditions demonstrates that the oxidized and micro-cracked surface layer becomes significantly more susceptible to material removal during sliding contact. The EDXS measurements performed inside the wear tracks further confirm this mechanism, showing a reduced oxygen concentration compared to the surrounding surface, which indicates that the wear process removes the oxidized layer generated during aging and exposes the less degraded subsurface material.

Taken together, these results suggest that UV radiation primarily induces surface photo-oxidation, while hygrothermal exposure enhances molecular mobility and structural rearrangement within the polymer matrix. The combined action of these mechanisms leads to progressive surface degradation and defect formation, which strongly influences tribological behavior while leaving the bulk mechanical properties largely unaffected.

5. Conclusions

In this study, FFF-printed PEEK specimens were subjected to ultraviolet (UV), hygrothermal (HT), and combined UV+hygrothermal (UV+HT) aging. Their chemical, morphological, mechanical, and tribological behavior was systematically investigated through FTIR, EDXS, SEM, tensile, hardness, and wear analyses. The results demonstrate that the different degradation mechanisms activated by UV radiation, hygrothermal exposure, and their combined action produce markedly distinct effects on the structure and properties of FFF-printed PEEK.

UV aging induces pronounced surface photo-oxidation. This chemical degradation is directly reflected in the surface morphology — micro-cracks, pores, and increased roughness — and leads to a drastic loss of wear resistance. However, the tensile response shows an unexpected increase in strength and elongation at break, suggesting that oxidation remains confined to the outermost layer without compromising the bulk structure, which instead appears to become more consolidated.

Hygrothermal aging produces less severe changes. FTIR analysis reveals structural chain rearrangement and enhanced crystalline order. As a result, a slight increase in elastic modulus and a substantial retention of tensile strength are observed, confirming the stabilizing effect of thermal treatment. At the same time, the increased crystallinity makes the surface more fragile under contact, reducing wear resistance. Therefore, hygrothermal aging can improve internal microstructural integrity while penalizing tribological performance.

The simultaneous exposure to UV and HT activates a synergistic degradation mechanism. FTIR shows the highest chemical complexity, while SEM reveals a heavily eroded and cratered surface. Despite this, tensile tests indicate the greatest increase in strength, modulus, and ductility among all aging conditions, suggesting that the surface degradation is accompanied by bulk molecular rearrangement and strengthening. Tribologically, however, the UV+HT condition results in the most severe wear, characterized by deep abrasion tracks and extensive surface failure. This clearly demonstrates that bulk mechanical properties are not predictive of wear performance in aged materials.

The results demonstrate that environmental aging affects the surface and bulk properties of FFF-printed PEEK in different ways. While the bulk mechanical response remains relatively stable, or even slightly improved, surface degradation caused by oxidation significantly compromises wear resistance. These findings indicate that, for engineering applications of FFF-printed PEEK exposed to aggressive environments, mechanical performance alone cannot be considered a reliable indicator of long-term tribological durability.

Therefore, in practical applications, the mechanical and tribological design of FFF-printed PEEK components should be considered separately. Specific post-processing or surface protection strategies may be required to preserve surface integrity while maintaining the favorable bulk mechanical properties of the material.

CRediT authorship contribution statement

Erica Billè: Conceptualization, Data Curation, Formal analysis, Investigation, Methodology, Project administration, Software, Validation, Visualization, Writing – original draft, Writing – review & editing. **Alessandro Gambitta:** Investigation, Resources, Writing – review & editing. **Alex Lanzutti:** Resources, Validation, Writing – review & editing. **Alfredo Rondinella:** Conceptualization, Investigation, Methodology, Resources, Validation, Writing – review & editing. **Francesco Sordetti:** Investigation, Resources, Writing – review & editing. **Marco Sortino:** Resources, Validation, Writing – review & editing. **Giovanni Totis:** Resources, Validation, Writing – review & editing. **Emanuele Vaglio:** Conceptualization, Formal analysis, Methodology, Project administration, Supervision, Validation, Writing – review & editing.

Declaration of competing interest

The authors declare that they have no known competing financial interests or personal relationships that could have appeared to influence the work reported in this paper.

Acknowledgments

Elettra-Sincrotrone Trieste and the Laboratory for Advanced Mechatronics–LAMA FVG–of the University of Udine are gratefully acknowledged for technical support. LAMA FVG is an international research center for product and process innovation where the three universities of Friuli Venezia Giulia (Italy) cooperate for promoting R&D activities at the academic and industrial level.

References

[1] Wang Z, Chen X, Chen X, Liang J, Zeng D, Gan Y. Effect of moisture content in polyether-ether-ketone (PEEK) filament on 3D printed parts. Discov Appl Sci 2024;6(8):394. http://dx.doi.org/10.1007/s42452-024-05963-6.

[2] Kurtz SM, Devine JN. PEEK biomaterials in trauma, orthopedic, and spinal implants. Biomaterials 2007;28(32):4845–69. http://dx.doi.org/10.1016/j.biomaterials.2007.07.013.

[3] Yao Y, He W, Li J, Gu J, Wu M, Ma H. Thermal-radiation aging on oriented poly (ether-ether-ketone) sheets. J Nucl Mater 2022;570:153948. http://dx.doi.org/10.1016/j.jnucmat.2022.153948.

[4] Tavlet M, van der Burgt H. Radiation resistance and other safety aspects of high-performance plastics by erta. Int Work Adv Mater High-Precision Detect 1994;157–67. http://dx.doi.org/10.5170/CERN-1994-007.157.

[5] Honigmann P, Sharma N, Okolo B, Popp U, Msallem B, Thieringer FM. Patient-specific surgical implants made of 3D printed PEEK: material, technology, and scope of surgical application. BioMed Res Int 2018;2018(1):4520636. http://dx.doi.org/10.1155/2018/4520636.

[6] Mylläri V, Ruoko T-P, Vuorinen J, Lemmetyinen H. Characterization of thermally aged polyetheretherketone fibres–mechanical, thermal, rheological and chemical property changes. Polym Degrad Stab 2015;120:419–26. http://dx.doi.org/10.1016/j.polymdegradstab.2015.08.003.

[7] Dua R, Rashad Z, Spears J, Dunn G, Maxwell M. Applications of 3D-printed PEEK via fused filament fabrication: a systematic review. Polymers 2021;13(22):4046. http://dx.doi.org/10.3390/polym13224046.

[8] Ahmad J, Niasar MG. Aging behavior of PEEK, PTFE, and PI insulation materials under thermal oxidative and humid conditions for aerospace applications. J Appl Polym Sci 2025;142(19):e56858. http://dx.doi.org/10.1002/app.56858.

[9] Sikder P, Challa BT, Gummadi SK. A comprehensive analysis on the processing-structure-property relationships of FDM-based 3-D printed polyetheretherketone (PEEK) structures. Materialia 2022;22:101427. http://dx.doi.org/10.1016/j.mtla.2022.101427.

[10] Arif M, Kumar S, Varadarajan K, Cantwell W. Performance of biocompatible PEEK processed by fused deposition additive manufacturing. Mater Des 2018;146:249–59. http://dx.doi.org/10.1016/j.matdes.2018.03.015.

[11] Greco A, De Luca A, Gerbino S, Lamanna G, Sepe R. Influence of infill pattern and layer height on surface characteristics and fatigue behavior of FFF-printed PEEK. Fatigue Fract Eng Mater Struct 2024;47(12):4741–54. http://dx.doi.org/10.1111/ffe.14450.

[12] Billè E, Franulović M, Gambitta A, Liović D, Rondinella A, Scalzo F, Sortino M, Totis G, Vaglio E. Experimental investigation on the effect of the fused deposition modeling parameters on the processing of polyether ether ketone. J Mater Res Technol 2025;36:8007–21. http://dx.doi.org/10.1016/j.jmrt.2025.04.295.

[13] Ouyang Z, Zhang Z, Jing Y, Bai L, Zhao M, Hao X, Li X, Guo X. The photo-aging of polyvinyl chloride microplastics under different uv irradiations. Gondwana Res 2022;108:72–80. http://dx.doi.org/10.1016/j.gr.2021.07.010.

[14] Yousif E, Haddad R. Photodegradation and photostabilization of polymers, especially polystyrene: review. Springerplus 2013;2:398. http://dx.doi.org/10.1186/2193-1801-2-398.

[15] Saad M, Bucki M, Bujok S, Pawcenis D, Rijavec T, Górecki K, Bratasz Ł, Cigić IK, Strlič M, Kruczała K. The impact of heat and humidity on unplasticized poly (vinyl chloride). Polym Degrad Stab 2025;238:111334. http://dx.doi.org/10.1016/j.polymdegradstab.2025.111334.

[16] Mao R, Lang M, Yu X, Wu R, Yang X, Guo X. Aging mechanism of microplastics with UV irradiation and its effects on the adsorption of heavy metals. J Hazard Mater 2020;393:122515. http://dx.doi.org/10.1016/j.jhazmat.2020.122515.

[17] Ainali NM, Bikiaris DN, Lambropoulou DA. Physicochemical alterations on UV aged polymers leading to microplastics formation: A multi-tiered study of polyester, polycarbonate and polyamide. Polym Degrad Stab 2024;222:110692. http://dx.doi.org/10.1016/j.polymdegradstab.2024.110692.

[18] Tocháček J, Vrátníčková Z. Polymer life-time prediction: The role of temperature in UV accelerated ageing of polypropylene and its copolymers. Polym Test 2014;36:82–7. http://dx.doi.org/10.1016/j.polymertesting.2014.03.019.

[19] Sun J, Zheng H, Xiang H, Fan J, Jiang H. The surface degradation and release of microplastics from plastic films studied by UV radiation and mechanical abrasion. Sci Total Environ 2022;838:156369. http://dx.doi.org/10.1016/j.scitotenv.2022.156369.

[20] Ho K-LG, Pometto III AL, Hinz PN. Effects of temperature and relative humidity on polylactic acid plastic degradation. J Environ Polym Degrad 1999;7(2):83–92. http://dx.doi.org/10.1023/A:1021808317416.

[21] Jiang H, Wang Y, Sun J, Mao Y, Que S, Lin Y, Huang Y, Lei X. The aging behavior of degradable plastic polylactic acid under the interaction of environmental factors. Environ Geochem Health 2024;46(5):163. http://dx.doi.org/10.1007/s10653-024-01932-5.

[22] Gupta A, Kumar N, Sachdeva A. Factors affecting the ageing of polymer composite: A state of art. Polym Degrad Stab 2024;221:110670. http://dx.doi.org/10.1016/j.polymdegradstab.2024.110670.

[23] Amza C, Zapciu A, Baciu F, Vasile M, Nicoara A. Accelerated aging effect on mechanical properties of common 3D-printing polymers. Polymers 2021;13:4132. http://dx.doi.org/10.3390/polym13234132.

[24] Amza CG, Zapciu A, Baciu F, Radu C. Effect of UV-c radiation on 3D printed ABS-PC polymers. Polymers 2023;15(8):1966. http://dx.doi.org/10.3390/polym15081966.

[25] Bergaliyeva S, Sales DL, Delgado FJ, Bolegenova S, Molina SI. Effect of thermal and hydrothermal accelerated aging on 3D printed polylactic acid. Polymers 2022;14(23):5256. http://dx.doi.org/10.3390/polym14235256.

[26] Courvoisier E, Bicaba Y, Colin X. Multi-scale and multi-technique analysis of the thermal degradation of poly (ether ether ketone). Polym Degrad Stab 2018;151:65–79. http://dx.doi.org/10.1016/j.polymdegradstab.2018.03.001.

[27] Nakamura H, Nakamura T, Noguchi T, Imagawa K. Photodegradation of PEEK sheets under tensile stress. Polym Degrad Stab 2006;91(4):740–6. http://dx.doi.org/10.1016/j.polymdegradstab.2005.06.003.

[28] de Seijas MOV, Piskacev M, Celotti L, Nadalini R, Daurskikh A, Baptista A, Berg M, Caltavituro F, Major I, Devine DM, et al. Closing the loop in space 3D printing: Effect of vacuum, recycling, and UV aging on high performance thermoplastics produced via filament extrusion additive manufacturing. Acta Astronaut 2024;219:164–76. http://dx.doi.org/10.1016/j.actaastro.2024.03.015.

[29] Zhu C, Zhang H, Li J. Thermal aging study of PEEK for nuclear power plant containment dome. J Polym Res 2022;29(1):5. http://dx.doi.org/10.1007/s10965-021-02839-w.

[30] Lin J, Yan D, Fu J, Chen Y, Ou H. Ultraviolet-c and vacuum ultraviolet inducing surface degradation of microplastics. Water Res 2020;186:116360. http://dx.doi.org/10.1016/j.watres.2020.116360.

[31] Sınmazçelik T, Yılmaz T. Thermal aging effects on mechanical and tribological performance of PEEK and short fiber reinforced PEEK composites. Mater Des 2007;28(2):641–8. http://dx.doi.org/10.1016/j.matdes.2005.07.007.

[32] Xu X, Zhang B, Shi F, Liu K, Peng G, Gao L, Gao J, Du Y. Study on the influence of hygrothermal aging on the mechanical properties of carbon fabric/polyetheretherketone composites. Polymers 2025;17(6):724. http://dx.doi.org/10.3390/polym17060724.

[33] El Magri A, Vaudreuil S. Effects of physical and chemical ageing on 3D printed poly (ether ether ketone)/poly (ether imide)[peek/pei] blend for aerospace applications. J Mater Sci 2023;58(3):1465–79. http://dx.doi.org/10.1007/s10853-022-08068-w.

[34] Abbas K, Balc N, Bremen S, Skupin M. Crystallization and aging behavior of polyetheretherketone PEEK within rapid tooling and rubber molding. J Manuf Mater Process 2022;6(5):93. http://dx.doi.org/10.3390/jmmp6050093.

[35] Miura D, Ishida Y, Shinya A. The effects of different molding orientations, highly accelerated aging, and water absorption on the flexural strength of polyether ether ketone (PEEK) fabricated by fused deposition modeling. Polymers 2023;15(7):1602. http://dx.doi.org/10.3390/polym15071602.

[36] Richaud E, Ferreira P, Audouin L, Colin X, Verdu J, Monchy-Leroy C. Radiochemical ageing of poly (ether ether ketone). Eur Polym J 2010;46(4):731–43. http://dx.doi.org/10.1016/j.eurpolymj.2009.12.026.

[37] Badeghaish W, Wagih A, Colin X, Hoteit H, Lubineau G. Effect of supercritical CO2 aging on the microstructure and mechanical properties of PEEK. Polym Degrad Stab 2025;233:111155. http://dx.doi.org/10.1016/j.polymdegradstab.2024.111155.

[38] Regis M, Lanzutti A, Bracco P, Fedrizzi L. Wear behavior of medical grade PEEK and CFR PEEK under dry and bovine serum conditions. Wear 2018;408:86–95. http://dx.doi.org/10.1016/j.wear.2018.05.005.

[39] International Standards Organisation. ISO 527-2:2012 - Plastics — Determination of tensile properties - Part 2: Test conditions for moulding and extrusion plastics,

[40] Sordetti F, Magnan M, Carabillò A, Querini M, Fedrizzi L, Lanzutti A. Influence of the surface finishing on the wear behaviour of cemented carbides worked by electrical discharge machining. Int J Refract Met Hard Mater 2023;113:106196. http://dx.doi.org/10.1016/j.ijrmhm.2023.106196.

[41] International Standards Organisation. ISO 2039-1:2001 - Plastics — Determination of hardness - Part 1: Ball indentation method. Available from: https://www.iso.org/standard/31264.html.

[42] Mylläri V, Ruoko T-P, Järvelä P. The effects of UV irradiation to polyetheretherketone fibres–characterization by different techniques. Polym Degrad Stab 2014;109:278–84. http://dx.doi.org/10.1016/j.polymdegradstab.2014.08.003.

[43] Rodzeń K, McIvor MJ, Sharma PK, Acheson JG, McIlhagger A, Mokhtari M, McFerran A, Ward J, Meenan BJ, Boyd AR. The surface characterisation of fused filament fabricated (FFF) 3D printed PEEK/hydroxyapatite composites. Polymers 2021;13(18):3117. http://dx.doi.org/10.3390/polym13183117.

[44] Gaitanelis D, Worrall C, Kazilas M. Detecting, characterising and assessing peek's and CF-peek's thermal degradation in rapid high-temperature processing. Polym Degrad Stab 2022;204:110096. http://dx.doi.org/10.1016/j.polymdegradstab.2022.110096.

[45] Al Lafi AG. FTIR spectroscopic analysis of ion irradiated poly (ether ether ketone). Polym Degrad Stab 2014;105:122–33. http://dx.doi.org/10.1016/j.polymdegradstab.2014.04.005.

[46] Zhao F, Li D, Jin Z. Preliminary investigation of poly-ether-ether-ketone based on fused deposition modeling for medical applications. Materials 2018;11(2):288. http://dx.doi.org/10.3390/ma11020288.

[47] Kuptsov A, Zhizhin G. Handbook of Fourier Transform Raman and Infrared Spectra of Polymers. Elsevier; 1998.

[48] Yang L, Ohki Y, Hirai N, Hanada S. Aging of poly (ether ether ketone) by heat and gamma rays—Its degradation mechanism and effects on mechanical, dielectric and thermal properties. Polym Degrad Stab 2017;142:117–28. http://dx.doi.org/10.1016/j.polymdegradstab.2017.06.002.

[49] Triminì V. Study and design of process parameters for additive manufacturing of PEEK and c-PEEK parts for aeronautical applications (Ph.D. thesis), Politecnico di Bari; 2025, https://doi.org/10.60576/poliba/iris/trimin-valentina_phd2025.

[50] Tang C-C, Chen H-I, Brimblecombe P, Lee C-L. Textural, surface and chemical properties of polyvinyl chloride particles degraded in a simulated environment. Marine Poll Bull 2018;133:392–401. http://dx.doi.org/10.1016/j.marpolbul.2018.05.062.

[51] Regis M, Bellare A, Pascolini T, Bracco P. Characterization of thermally annealed PEEK and CFR-PEEK composites: Structure-properties relationships. Polym Degrad Stab 2017;136:121–30. http://dx.doi.org/10.1016/j.polymdegradstab.2016.12.005.

[52] Lee A, Wynn M, Quigley L, Salviato M, Zobeiry N. Effect of temperature history during additive manufacturing on crystalline morphology of PEEK. Adv Ind Manuf Eng 2022;4:100085. http://dx.doi.org/10.1016/j.aime.2022.100085.